# Chapter 2

# Nanoimprint Lithography

## 2.1 INTRODUCTION

Electron beam lithography is not only the workhorse in research when pattern sizes in the sub-100-nm range are envisaged; it is also the current technique for optical mask fabrication for device production of pattern sizes of 1-2 μm and below. Moreover, it is the only production-proven technique for pattern sizes beyond optical lithography. Shaped beam techniques have been developed in order to increase productivity, where writing speed and writing fields of production systems have been improved substantially. Furthermore, projection systems such as SCALPEL (scattering with angular limitation projection electron beam lithography) have been developed where contrast is obtained by scattering of electrons out of the optical system [1]. Nevertheless, electron beam lithography is a technique with limited throughput, leading to high costs in device production. The contest of lithography techniques for reliable fabrication of future integrated nanometer-scaled devices is not yet settled.

In order for progress to be made, enabling nanofabrication techniques as tools for experiments to understand the underlying science and engineering in the nanometer scale, easily accessible and flexible nanofabrication approaches are required. Alternative techniques to cost-intensive or limited-access fabrication methods with nanometer resolution have been under development for nearly two decades. The literature on the subject is increasing very rapidly and recent reviews on progress in micro-contact printing [2, 3] and nanoimprint-based lithography (NIL) techniques [4],

have been published.

Richard Feynmann's famous sentence "There is plenty of room at the bottom" was visionary. His line of discourse led to the suggestion "We would press the metal into a plastic material, make a mold of it, then peel the plastic off very carefully, evaporate silica onto the plastic to get a very thin film, then shadow it by evaporating gold at an angle against the silica…These comments were based on his knowledge of existing technologies in the late 1950s. LIGA, hot embossing and, later on, nanoimprinting, followed. The underlying philosophy of alternative lithography is illustrated in Figure 2-1.

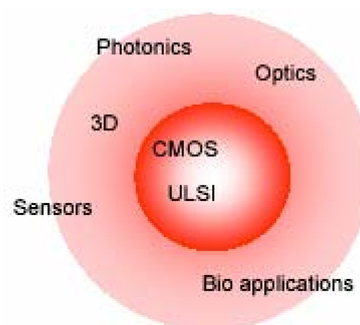


**Figure 2-1.** Connection between applications which have led developments in lithography, such as CMOS and ultra large scale integration, and a range of applications with probably less demands on the fabrication process such as those outside the front end of the CMOS process, the fabrication needs of which can be successfully covered by emerging lithographic methods. (Courtesy of J. Ahopelto).

### *2.1.1 Nanoimprint Lithography*

The term "nanoimprint lithography" was introduced by Chou in 1995 [5, 6]. It makes use of the mechanical deformation of a polymer layer under pressure and elevated temperature. The idea of the process is explained in Figure 2-2. The mold with its patterned surface and a sample, prepared with a layer of poly(methyl methacrylate) (PMMA), are heated up to about 200℃. Then, the stamp is pressed against the sample with a pressure of about130 bar. After cool-down to near 100℃,

the pressure is released and the mold is separated from the sample. The resulting patterned polymer forms a mask on the substrate.

The main advantages expected in comparison to electron beam writing are the parallel nature of the process, the high throughput, and the low system costs, because

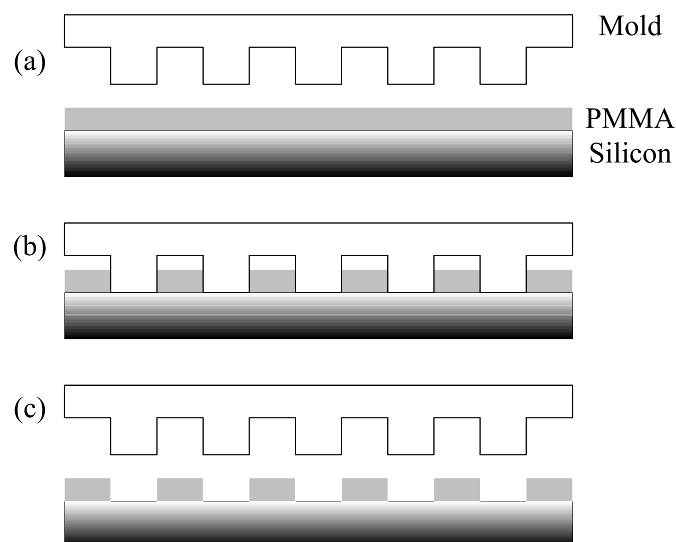


**Figure 2-2.** Principle of nanoimprint lithography or hot-embossing lithography. A patterned stamp and a Si wafer prepared with PMMA are heated to a temperature above the glass transition of the polymer (a); under pressure application, the polymer layer is patterned mechanically (b), resulting in a polymer mask on top of the wafer (c).

no energetic particle beam generator is needed [7, 8]. In addition, nanoimprinting eliminates a number of adverse effects of conventional lithography techniques [6, 8] such as wave diffraction, scattering and interference in the resist, electron backscattering from the substrate, and chemical issues of resists and developers. Large-area processing over more than 50 x 50 $mm^2$ is expected to work without the defect problems of state-of-the-art lithography [6]. Low-cost mass production of nanometer-scaled features can be achieved by multiple imprint, where only the mold has to be fabricated in a high-resolution, low-throughput process [8]. The resolution of NIL is determined by the mechanical strength of the mold and polymer. Using silicon-dioxide mold and PMMA resists (the glass transition temperature of 100 C),

the holes of 6 nm diameter (60 nm deep) in PMMA and the PMMA pillars of 30 nm diameter (35 nm tall) have been achieved using NIL [6, 9] (Figures 2-3).

This technique is also known as hot-embossing lithography [10] and is expected to be a powerful nanomanufacturing technique for the future, in particular, when resist structures with high aspect ratio are needed [11].

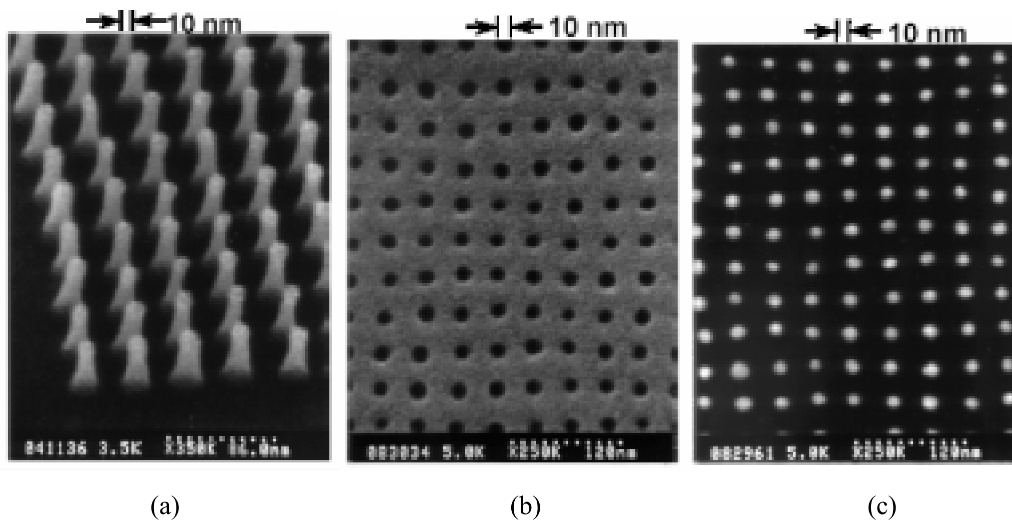


(a) (b) (c)

**Figure 2-3.** (a) SEM micrograph of a $SiO_2$ mold with 10 nm minimum diameter pillars with a 40 nm period which are 60 nm tall, after being used 12 times. (b) SEM micrograph of a top view of 60 nm deep holes imprinted into PMMA which have a 10 nm minimum diameter and a period of 40 nm. (c) SEM micrograph of a top view of 10 nm minimum diameter metal dots with a period of 40 nm, formed by imprinting into PMMA and a lift-off process.

### *2.1.2 Mold-Assisted Lithography*

Mold-assisted lithography was introduced by Haisma and coworkers in 1996 [12] and is based on the molding of a monomer in a vacuum contact printer and subsequent curing by ultraviolet (UV) radiation. The idea is illustrated in Figure3-4.

For a lithography process, UV curing has to be performed through the mold, which is therefore made from fused silica. The polymer layer features a thickness contrast after the process, and a thin residual layer has to be removed in a reactive ion

etching (RIE) step to form the local polymer mask. To prevent sticking during polymerization, the master and the substrate are treated with a mold release layer and a primer, respectively.

A major advantage of this process is its direct compatibility with current Si technology, as a commercially available vacuum contact printer is employed, enabling wafer-scale processing. Commonly used fused silica photomasks are the ideal choice for the master and UV radiation of 300-400 nm is used for curing. Thus, mold-assisted lithography should be a low-cost technique because no specific new tool development is required.

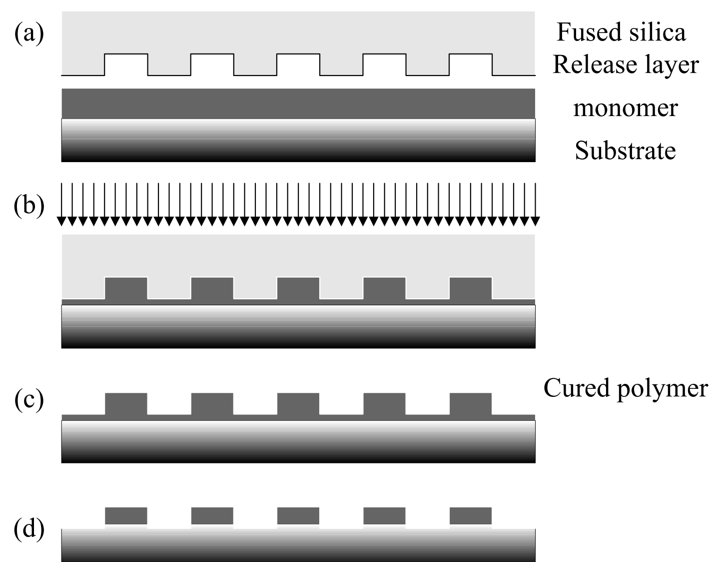


**Figure 2-4.** Principle of mold-assisted lithography. A fused silica mold is pre-pared with a release layer, the substrate with a primer and a monomer (a) Under vacuum contact, the monomer fills the mold cavities and is then cured by UV radiation (b). The thin residual layer of polymer remaining between the patterns after separation (c) is removed by etching, resulting in the polyrner mask (d).

## 2.2 HOT-EMBOSSING LITHOGRAPHY (HEL)

### *2.2.1 History of Classical Hot Embossing*

Embossing is the main technique for the fabrication of large-area holograms [13], in particular, relief phase holograms. The resolution required is 100 nm in depth and

several 100 nm laterally. Replication is accomplished with a metallic mold, which is heated and then embossed into a transparent material, typically a vinyl tape or sheet.

Embossing is also widely used for volume production of optical components [14]. Typical process parameters are temperatures of 140℃ and pressures of 30 bar, and typical patterned areas can reach up to 1000 $cm^2$. Another early example is the embossing of optical wave-guides in PMMA [15] using a glass fiber as the embossing tool. After filling of the embossed groove with a monomer and subsequent curing, the optical waveguide is completed.

### *2.2.2 Principle of Hot-Embossing Lithography*

Reviewing the literature and collecting the main ideas, the principle of hot embossing as a lithography process can be summarized according to Figure 2-5.

A mold with a patterned surface- the "stamp"- is prepared by state-of-the-art Si technology, for example, electron beam writing of small patterns into a resist followed by dry-etch pattern transfer into the substrate. This stamp is pressed into a thin polymer layer spun onto a substrate. The embossing is carried out at a temperature well above the glass transition temperature ($T_g$) of the polymer, where it has a relatively low viscosity and can flow under force. Suitable polymers should be thermoplastic ones moldable at elevated temperatures, with a $T_g$ around 100℃. Typical process temperatures are about 200℃ and typical pressures are about 100 bar. To separate the stamp from the sample, both are cooled down under pressure until the temperature is below $T_g$.

For easy separation of stamp and sample after imprinting, the polymer should feature good adherence to the substrate and substantially lower adherence to the stamp.

The initial thickness of the polymer layer has to be tuned to the pattern sizes, their fill factor, and the depth of the pattern relief in the mold. As soon as the stamp is in full

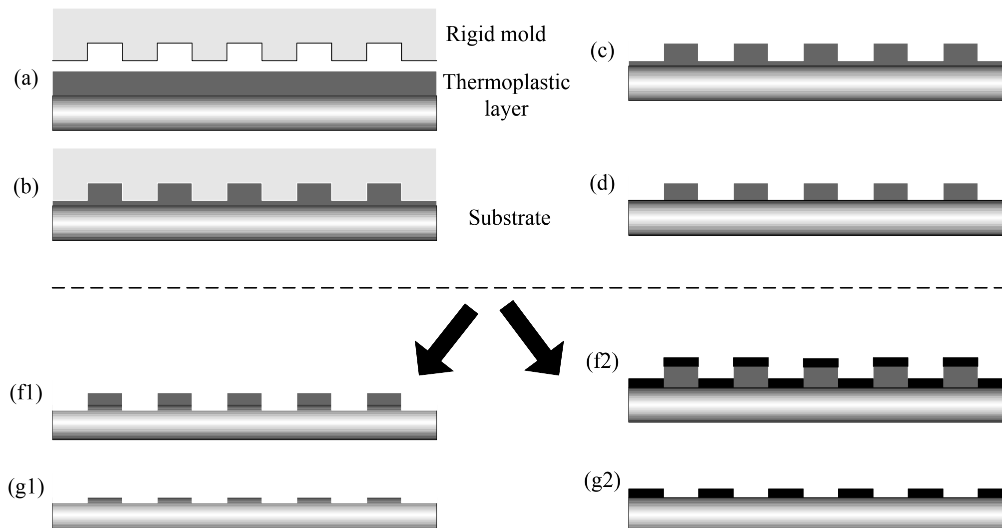


**Figure 2-5.** Schematics of patterning by use of hot-embossing lithography. Lithography comprises steps (a)-(e), whereas steps (f) and (g) refer to the subsequent processing with the HEL mask. (a) Sample (substrate with or without additional layer, covered with a thermoplastic polymer) is heated to T > $T_g$, together with a patterned rigid stamp; (b) stamp and sample are brought into contact; (c) polymer imprint via pressure application; (d) imprinted sample after cooldown and separation; (e) sample with polymer mask after residual layer removal. Left branch (with additional layer), dry etching: (fl) dry etch of additional layer with the polymer mask; (gl) patterned layer after mask stripping. Right branch (no additional layer), lift-off: (f2) evaporation of metal over masked sample; (g2) patterned metal on top of substrate after polymer dissolution in solvent. The lift-off pattern is negative compared to the patterned additional layer of (gl).

area contact with the polymer, which is the case when the polymer fills the whole stamp relief pattern conformally, the effective pressure decreases and the imprint "stops." In fact, it slows down as a consequence of polymer transport phenomena.

A residual layer of polymer remains within the compressed regions. This residual layer protects the rigid master from contact with the hard substrate and thus prolongs the lifetime of the stamp [8]. When a lithography process is envisaged, this residual layer has to be removed in order to result in a polymer mask on top of the substrate.

This is generally done in an anisotropic RIE step in oxygen. To minimize the demands for this dry-etch step, the residual layer thickness after embossing should be small in comparison to the pattern height achieved in the imprinted polymer. After RIE, the lithography is completed and the polymer mask can be used for further processing of the surface. Pattern transfer of the mask into the underlying layer or in the substrate itself is performed by etching, preferably by RIE, as this is the only technique suitable for pattern transfer in the nanometer range. When layer patterning is envisaged, the

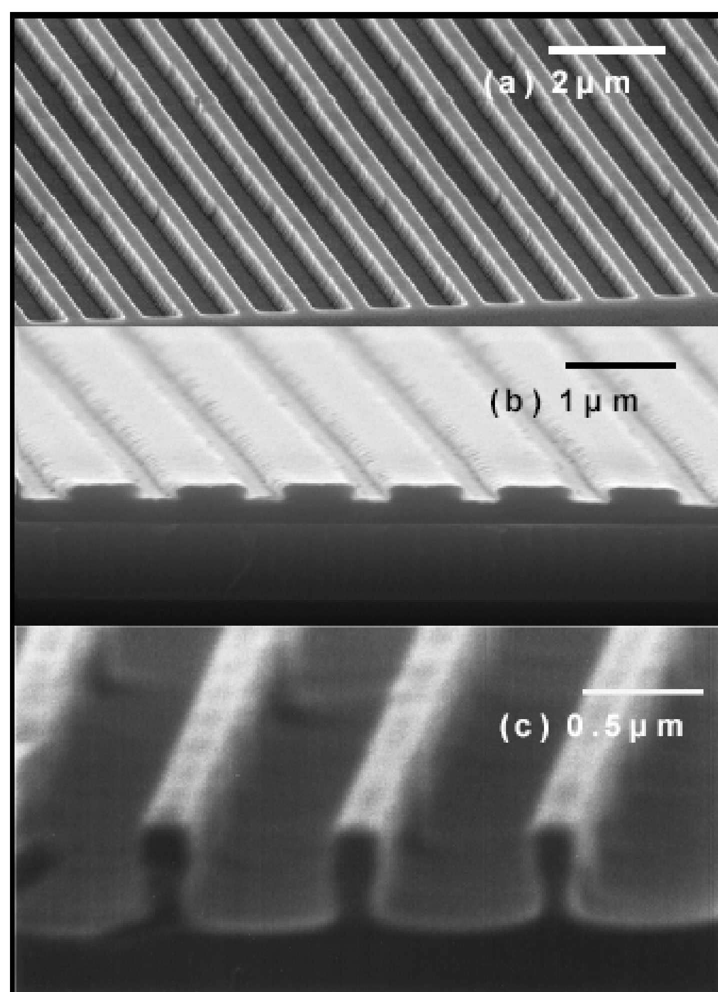


**Figure 2-6**. SEM micrographs of: (a) the Si stamp with 800 nm period used to print the structure in (b); (b) printed PMMA on GaAs and (c) GaAs wires after dry etching using PMMA NIL patterning and lift off, the wire width is approximately 200 nm. (Courtesy of M. V. Maximov)

substrate has to be covered with the respective layer before spinning the polymer (left branch of Figure 2-5). In case of lift-off (right branch of Figure 2-5), the surface of the

patterned polymer is covered with a thin layer (e.g. a metal) preferably by evaporation. Due to the low pressure regularly involved in this step, the metal atoms travel straight to the sample without scattering with the background gas. As a consequence, the evaporated layer will not cover the pattern slopes as long as they are sufficiently steep and the aspect ratio is high enough. Dissolution of the polymer will then remove the metal deposited on the polymer and a patterned metal film remains on the substrate surface. Typical large-area imprinted feature are shown in Figure 2-6.

### *2.2.3 Embossed Materials*

Most of the hot-embossing experiments have been performed in PMMA, a well-known e-beam resist. This material is available in a broad range of molecular weights. It is a thermoplastic polymer, which softens and flows with increasing temperature. Its glass transition temperature is 105°C.

PMMA is reported to be a good choice in combination with a mold from $SiO_2$, because the polymer has a hydrophilic surface [7] and will not stick to the stamp. Its thermal expansion coefficient is $5\text{x}10^{-5}K^{-1}$, and its pressure shrinkage coefficient is $5.5 \text{ x } 10^{-6} \text{ bar}^{-1}$, so that the thermal shrinkage is below 0.8 % and the pressure shrinkage below 0.07% within a typical cooldown step [8, 16].

Excellent polymer flow is reported for 15 k PMMA (PMMA with a mean molecular weight of 15 kg/mol) at quite low temperature and pressure (175°C, 45 bar) [17], and a low-molecular-weight polymer (50 k PMMA) displays much better flow than one with a high-molecular-weight (950 k) [18]. This supports theoretical expectations with respect to changes of viscosity for different molecular weights.

PMMA also offers preparation advantages. Solved in chlorobenzene, it lends

itself to spin coating free from surface nonuniformities, which could be caused by local density fluctuation or highly volatile solvent [19]. Imprinting in AZ and Shipley novolack resin-based resists is mentioned to be suitable but no details have been given [15]. New polymers optimized for nanoimprinting have been reported, featuring better mask selectivity than PMMA in a fluorine-based dry-etch process [20-21]. This is a result of including aromatic groups in the resist formulation. Their imprint behavior is excellent [20] and they show even less sticking to $SiO_2$, than PMMA.

In addition, highly polar copolymers were tested for imprint, featuring a light network due to H bonding, which is degradable at elevated temperatures. These polymers had to be imprinted using a specific procedure schematically shown in Figure 2-8.

### *2.2.4 Processing Details*

Typical process data for hot-embossing lithography include a pressure of 40-100 bar and a temperature 50-100℃ above the glass transition temperature $T_g$ of the polymer. Whereas the first publications reported quite high values of 200 ℃ and 130 bar [5, 7, 8, 16], values of 175℃ and 45 bar became a standard for the imprint of PMMA [17, 18, 22].

In most cases, both the stamp and the sample are heated to the imprint temperature, and then pressure is applied and held during the cooldown step until a temperature below $T_g$ is reached. Figure 2-7 (top) shows this standard procedure. Maintaining the pressure during the cooling phase is a critical point for successful pattern definition. The parameter "embossing time" $t_{emb}$ is not clearly defined. Often the time at full pressure and highest temperature is meant (full line arrows in Figure 2-7), but a certain percentage of the cooldown time (or heating time) under pressure (a

certain minimum level above $T_g$) will be efficient, too, for local polymer transport This is of concern, in particular, in cases where heating and/or cooldown times under pressure are long compared to the holding time (time at highest temperature).

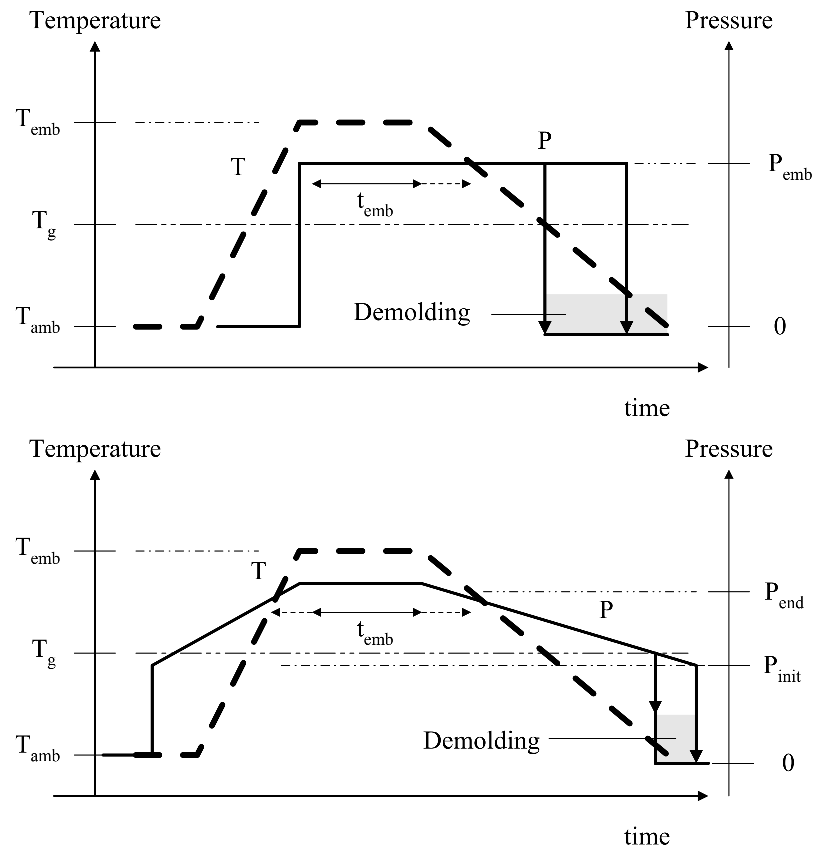


**Figure 2-7.** Schematics of typical processing sequences during hot embossing used in conjunction with hydraulic systems with heating-cooling lines (top) and simple clamp devices put into an oven (bottom). Note that a constant pressure is only achieved under pressure control as long as the temperature of the system changes.

Demolding, the separation of stamp and sample, is recommended around $T_g$ where polymers react soft-elastically to mechanical stresses by conformational changes in order to prevent damage to the embossed pattern during separation. This is only possible in systems where the sample and the stamp are fixed to the stages and in which pressure release and demolding are coupled. In simple systems, this is often not the case and demolding has to be performed manually [23]. This might require application of shear forces (e.g., via a scalpel). The demolding step is critical and can

lead to extended damage of the stamp [24] and of the polymer film, in particular, for structures with high aspect ratio.

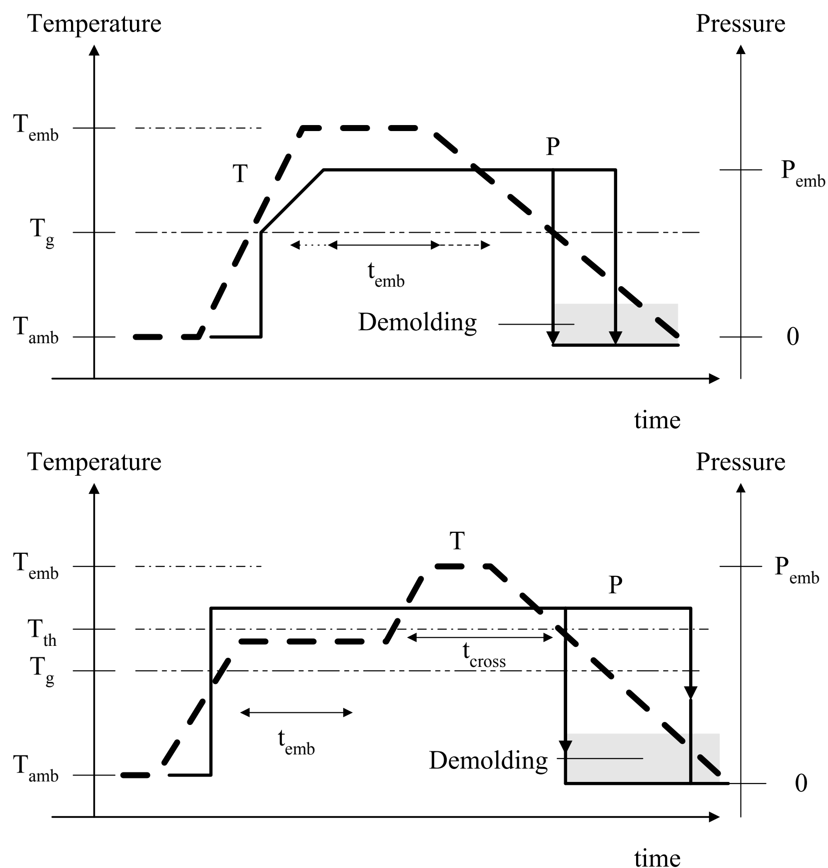


**Figure 2-8.** Schematics of processing sequences used for hot embossing of thermally modified (MAA/MA) copolymers (top) and crosslinkable polymers (bottom).

Two types of crosslinked or crosslinking polymers have been investigated. The first type refers to MAA/MA (methyl methacrylate/methacrylic acid) copolymers where the highly polar acid groups form a weakly bound network via H bonding, thus tailoring $T_g$ [25]. At about 180℃, adjacent acid groups may form anhydrides, leading to a loss of polarity, a decrease in H bonding, and thus a decrease in $T_g$, which should lower the viscosity and thus improve the embossing quality at a temperature above 180℃. This could not be confirmed in the experiments, most probably because the effect is too weak during typical imprint times. However, it could be shown that for

such lightly crosslinked polymers an improvement in the embossing quality can be achieved when pressure is applied from $T_g$ on. Using a modified procedure as shown in Figure 2-8 (top), the definition of patterns from 400 nm up to 10 μm was improved substantially. In addition, the gradual increase in pressure also resulted in a reduction in the observed sticking between stamp and sample.

The second type of investigated polymers is thermosets where a crosslink is initiated by thermal treatment. This causes a behavior opposite to the one described for the first polymer type. Above the threshold, the viscosity increases with increasing temperature.

Thermosets have shown high etch resistance and thus good mask selectivity in a dry-etch process subsequent to hot-embossing lithography [26], and they have high thermal stability in their crosslinked duroplastic state [27]. The polymers developed and investigated for hot embossing feature a crosslink threshold of about 120℃. They are embossed in their thermoplastic prepolymer form. Typical glass transition temperatures are around 70℃. Up to 120℃, they can be imprinted using the standard process of Figure 2-7 (top). When higher temperatures are applied for embossing, the full time the polymer remains viscous has to be used in order to achieve sufficient polymer flow before the crosslinking process increases the polymer $T_g$, and decreases viscosity, thus inhibiting pattern transfer. In this case, pressure should again be applied from $T_g$ on according to Figure 2-8 (bottom) [21], and in the case of high heating rates, it should be sustained for some time at a temperature slightly below the crosslinking threshold to enable flow.

## 2.3 MASTERS, STAMPS, AND MOLDS

Classical lithography can only work successfully when three prerequisites are

fulfilled. There has to be (i) a mask technology providing the original patterns, (ii) a polymer sensitive to exposure at the respective wavelength, and (iii) the exposure system with the lithography process itself [1]. These three prerequisites have to fit together and the mask technology is often a critical part [28]. Mask requirements differ to a large extent and include the phase-shifting masks for advanced optical lithography, the transmission masks for X-ray lithography, the reflection masks for EUV, the stencil masks for IPL, and the scattering masks for electron beam projection (SCALPEL). Direct writing techniques are the only ones scoping the mask problem, but as serial techniques they have to face the throughput issue.

Thus, the need for a master with the envisaged pattern is a general aspect of broad-beam lithography techniques and not specific to nanoimprinting. Moreover, as in any lithography process, the achieved quality is directly related to the mask quality where distortion, defects, and particle contamination are crucial. In cases of demagnifying exposure systems, the demands for pattern accuracy are slightly relaxed as is the case for SCALPEL, EUV, or IPL, where 4 : 1 masks are supposed [1] similar to state-of-the-art optical lithography. X-ray lithography with its 1 : 1 masks is comparable to nanoimprint lithography as far as pattern accuracy is concerned.

### *2.3.1 Master Fabrication*

Mold for nanoimprint techniques are fabricated in most cases using state-of-the-art Si technology. Nanometer-scaled patterns are e-beam written into a resist layer on a substrate as is common for mask fabrication in today's advanced lithography. When, in addition, larger pattern sizes are required over large areas, a mix and match with UV lithography may be the choice.

In many cases, the patterned polymer layer on a quartz substrate or on a Si wafer

is not robust enough to serve as a mold during the imprint process. In these cases, transfer of the polymer pattern into the underlying layer or substrate is required. This is done by dry etching (RIE). Often the pattern is transferred into quartz or into a $SiO_2$ layer on Si [5, 9, 29] or, alternatively, into poly-Si over oxide on Si [21, 23, 25] or into bulk Si [10, 24]. Standard dry-etch processes used for contact hole etching or gate etching can be used in this step. Different types of stamps are shown in Figure 2-9.[29]

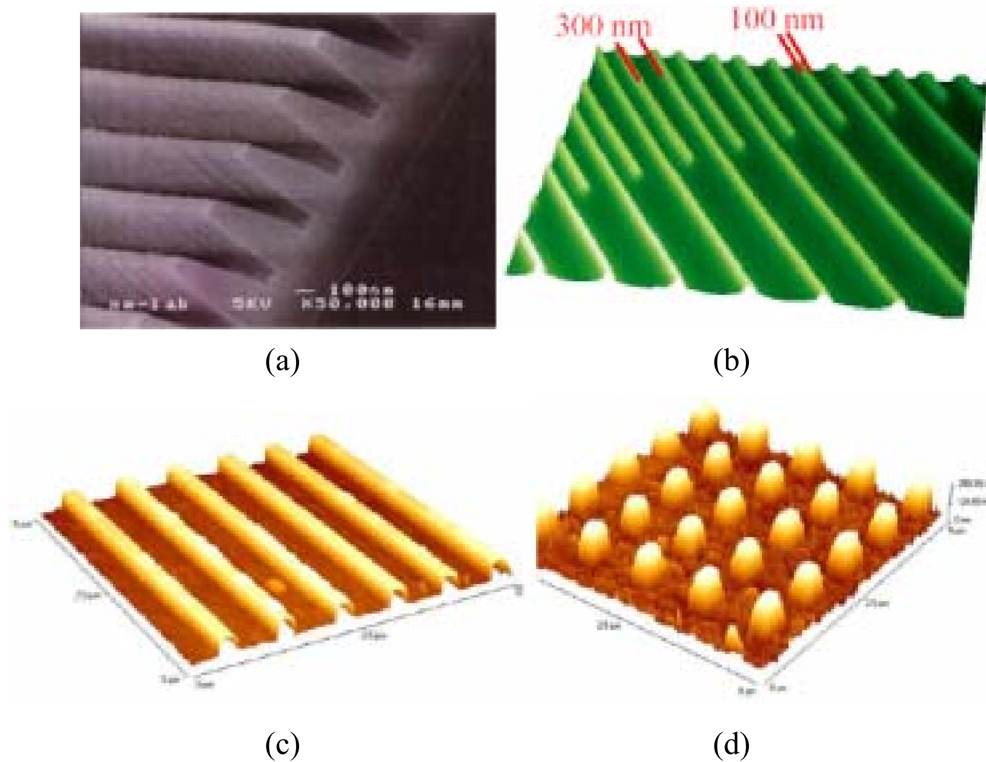


**Figure 2-9.** (a) 100 nm lines and 300 nm spacing in $SiO_2$ The height of the structures is 300nm.(b) AFM of a Nickel stamp made according to description as above. (c), (d) Aluminum structures on $SiO_2$. The thickness of the metal is 200 nm.

### *2.3.2 Polymer Masters*

An alternative for low-cost master fabrication is direct e-beam writing into a solid polymer sheet of, for example, perspex (PMMA) [30]. To minimize charging effects during exposure, the plastic is covered with a 30-nm NiCr layer in a low-temperature-load evaporation process before writing. It can serve as a stamp for

hot embossing up to temperatures around its $T_g$ where the polymer is still glassy. Such rigid stamps from plastic offer elastic response without viscous flow in the time regime of the imprint process and could thus reduce the danger of damage in case of contact between stamp and sample substrate toward the end of the imprint process which is, in general, carefully avoided [16]. In combination with high-aspect-ratio stamp patterns, hot-embossing lithography of thin low-$T_g$ polymer layers could thus be feasible with minimum residual layer thickness over large areas.

In a different approach, a commercial crosslinkable resist (SU-8) is used for e-beam direct writing of a mold. In this case, a thin layer of the resist on 10-nm Cr on Si is used. The polymer is cured in the e-beam, and the patterns so formed result in a temperature-stable stamp for hot embossing.

## 2.4 STICKING EFFECT

As all imprint techniques rely on contact between stamp and sample, the wetting and adhesion characteristics of the polymer materials to the substrate, on the one hand, and to the stamp or mold, on the other hand, are critical issues.

Sticking effects will reduce the lifetime of stamps and molds, limit the quality of the replication, and complicate the processing procedures. For reliable processing, sticking has to be eliminated by choice of appropriate preventive measures. This may require the help of antiadhesive layers.

### *2.4.1 Physics of Adhesion*

During separation of two materials, the "internal" surface of their interface is transformed into two "external" surfaces interfacing with air. Assuming $\gamma_p$ and $\gamma_s$ are

the surface energies of the polymer and the substrate in air and $\gamma_{PS}$; the surface energy, of the intact interface, then the adhesion energy $W_{adh}$ is simply given by the surface energy difference between the two states [31], the intact one $W_{int}$ and the separated one $W_{sep}$ as

$$W_{adh} = W_{sep} - W_{\text{int}} = (\gamma_p + \gamma_s) - \gamma_{ps} \quad (1)$$

Thus, knowledge of the strength of adhesion requires knowledge of the surface energies of the involved materials and the respective interface.

For a liquid, the surface energy is identical to the well-knowledge parameter surface tension. In the case of solid materials, surface energies are determined by contact-angle measurement and numerous values energies are available from the literature (e.g., [32] for polymers). Typical values for standard polymers lie in the range of 30-40 mJ/m$^2$ [PMMA, 41.1mJ/m$^2$, polystyrene (PS), 40.7 mJ/m$^2$]. Commercial Teflon (PTFE) and PDMS are low-surface-energy materials with values of 20 and 21.6 mJ/m$^2$, respectively. Surface energies of oxides (silica) depend on the specific preparation and amount to about 70 mJ/m2 [31] (wetting angle 20°).

Values of the surface energy of interfaces are often derived from measurements of the adhesion energy $W_{adh}$ according to Eq. (1). When no measurements of $W_{adh}$ exist but when the surface energies of the materials in contact are known, an estimate following [32] is possible. The authors assume for the interfacial surface energy:

$$\gamma_{ps} = \gamma_p + \gamma_s - 2C\sqrt{(\gamma_p \gamma_s)} \approx \left(\sqrt{\gamma_p} - \sqrt{\gamma_s}\right)^2 \text{ for C=1} \quad (2)$$

with C as a constant, leading to an expression for the adhesion energy, which requires the surface energies only [33]:

$$W_{adh} \approx \gamma_p + \gamma_s - \left(\sqrt{\gamma_p} - \sqrt{\gamma_s}\right)^2 \qquad (3)$$

This approximation is often used for polymer.

### *2.4.2 Surface Energy Measurement*

As mentioned previously, surface energies of solid materials are measured via the contact angle method. Definite droplets of at least two liquids of different known surface tension (surface energy) are placed on the solid surface and the developing "contact angles" δ of the liquids are measured (see Figure 2-10). Values $\delta < 90°$ refer to a wetting situation, whereas values $\delta > 90°$ refer to a dewetting situation, where δ is measured from the solid surface inside the droplet. Often the measurement systems are designed for specific test liquids. In general, one of the liquids is water; the others may be diiodomethane ($CH_2I_2$), and glycerol [31, 34]. The basic measurement relies on an equilibrium between solid, liquid, and air, which can be described by Young's equation [32, 35]:

$$\gamma_L \cos\delta = (\gamma_S - \gamma_{SL}) - (\gamma_S - \gamma_{SV}) \approx (\gamma_S - \gamma_{SL}) \qquad (4)$$

where $\gamma_L$ is the known surface tension of the test liquid, $\gamma_s$ the unknown surface energy of the solid, and $\gamma_{SL}$ and $\gamma_{SV}$ a the interfacial energies of the solid surface to the liquid and to air. In general, the second term in parentheses is near zero and may be omitted, resulting in the previous approximation. Contact-angle measurements have to supply at least two data points ($\delta_1$, $\gamma_{L1}$; $\delta_2$, $\gamma_{L2}$), which are used for an extrapolation toward ideal (complete) wetting. In the case of complete wetting, δ will tend to zero (thus, $\cos \delta = 1$) and the interfacial energy between solid and liquid $\gamma_{SL}$ tends to zero. In this case, Eq. (4) is reduced to $\gamma_L = \gamma_S$ so that y; can be deduced from extrapolation of the cosδ data to complete wetting. The extrapolation idea is illustrated in Figure

2-10. The curve cosδ against $\gamma_L$ follows approximately a hyperbolic law as indicated by Eq. (4). Historically, plots of $\gamma_L \cos\delta$ vs. $\gamma_L$ were also used for extrapolation [33].

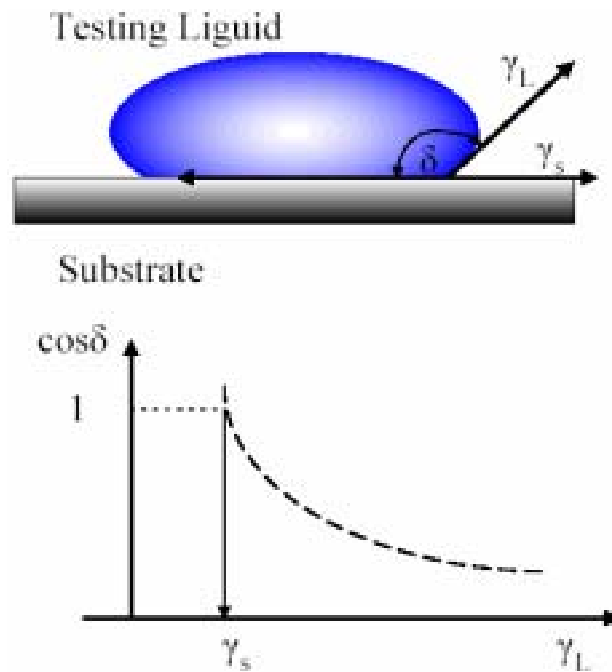


**Figure 2-10**. Contact-angle definition and principle of determination of surface energy from measurements with test liquids of different surface tension.

### *2.4.3 Antisticking Layers*

As an antisticking layer for hot embossing and molding, the search is for a few monolayers of a chemically inert material that is easy to apply uniformly and conformally over the patterned surface of the stamp or mold. It should feature minimum wear during imprint so that a large number of replications can be performed without cleaning and, in particular, without renewal of the layer. As such layers should have (i) antiadhesive properties to prevent bonding in general and (ii) lubricating properties to facilitate gliding and to reduce friction effects in the case of HEL.

Self-assembly is a widely used phenomenon for realizing very thin and homogeneous layers on top of a substrate. In general, amphiphilic linear aliphatic

chain molecules are used, featuring a head group at one end, which provides the functionality of the final surface layer, such as wettability, adhesion, or lubrication [36], and a base group at the other end, which provides a chemical link to the surface. The chain length determines the thickness of the self-assembled monolayer. The chains have to feature a regular conformation to enable defect- free two-dimensional assembly at the surface. This prerequisite is fulfilled for the commonly used $-(CH_2)_n$ chains.

When self-assembled layers are used for anti-sticking purposes, silica and silica-like materials (Si, metals, and their oxides) are the substrates of interest. Stamps and molds-are often fabricated from $Si/SiO_2$, SAM ASLs have been tested for mold assisted lithography [12, 31] as well as for hot-embossing lithography [37, 38].

Typically, the layers are prepared by immersion of the substrate at room temperature into a water-free solution of the SAM material [38]. Alternatively, deposition from the gas phase at elevated temperatures (>300 °C) is possible but only short chain SAMs have a high enough vapor pressure for this preparation [39,40].

For chemical anchoring of the chains to a silica surface, chlorosilane base groups ($-Si_nHCl_{3-n}$) are used. The most popular alkylsiloxane is OTS (octadecyl-tri-chlorosilane, $CH_3-(CH_2)_{17}-SiCl_3$), consisting of a chain of 18 C atoms with a triclorosilane group at the end [38, 41]. Due to its chain length, a dense self-assembled layer of OTS has a thickness of 22 Å [42].

Silica surfaces are unless prepared under specific high-temperature and low-pressure conditions where the -OH groups condense and are removed from the surface in a process called dehydration. Due to their polarity, the -OH groups tend to adsorb water; thus, they are hydrophilic. This water film can comprise one or more

monolayers and is crucial for anchoring of the chlorosilane group to the surface.[40, 41-44]

Layer formation is suggested to proceed in the following three steps [44] illustrated in Figure 2-11: (i) physical adsorption of the SAM to the previously formed water film at the solid surface, (ii) hydration of the chlorosilane groups where the Cl atoms are exchanged by OH groups under reaction with water to HCI, and (iii) polymerization of the SAM at the surface where the siloxane molecules become linked together laterally via -O atoms under formation of water (dehydration) and where also a few links to the surface are built up.

This model is supported by the finding that the SAM layer has a lower roughness than the substrate surface. In addition, it can be proven by Fourier transform infrared spectroscopy (FTIR) measurements that the hydrolyzed silica surface remains nearly unchanged during SAM formation and that only a few surface bonds are formed [41, 43].

The SAM coverage depends on the number of -OH groups at the silica surface but complete hydration is not necessary for complete coverage of the surface [43]. On the contrary, a thick water layer gives rise to a polymerized SAM layer without surface bonds sitting on top of the surface water so that it can easily be floated off [40]. In the extreme case, bulk polymerization occurs in the solvent, manifesting itself as particulates at the surface [45]. As the hydration of the surface is a critical factor, it might be advisable to dehydrate the samples as mentioned previously. At temperatures from 170 to 400°C, the silanol groups at the surface condense and eliminate water. Within this temperature range more than 50% of the -OH groups will remain. Under such conditions, the process is reversible, and rehydration starting from these -OH groups is easily performed in room temperature water within several minutes [43].

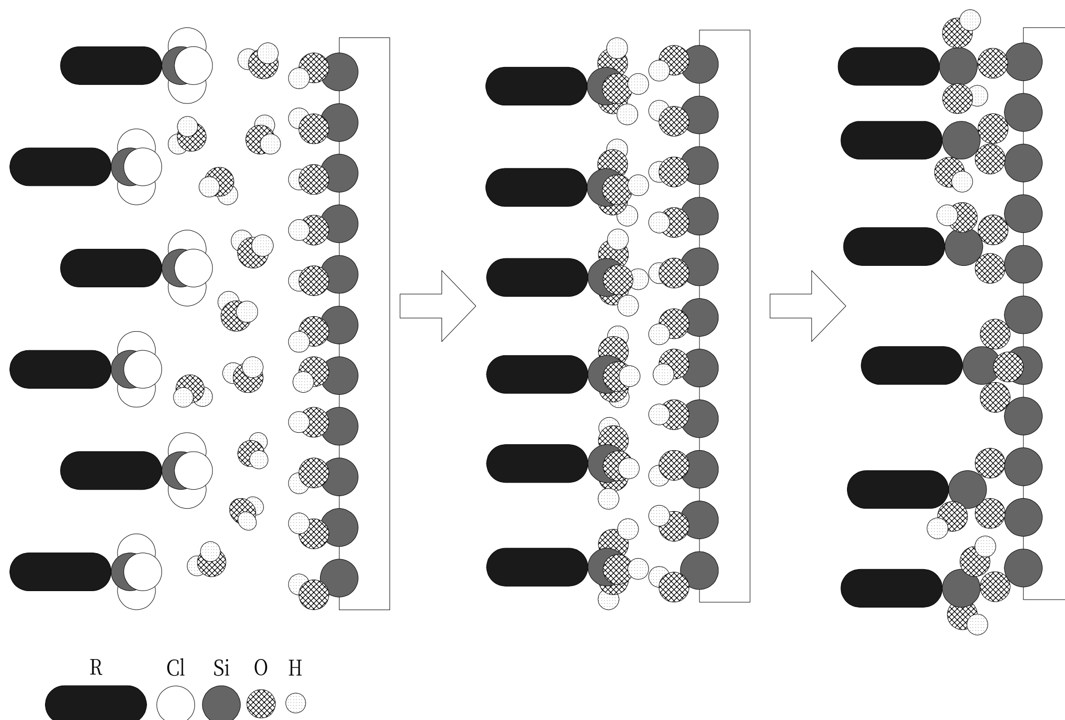


**Figure 2-11**. Illustration of the formation of a self-assembling crosslinked siloxane layer on Si as a three-stage process as supported by [44]: physical adsorption to the OH-terminated Si covered with surface water (a), hydration of the siloxane under HCl formation (not shown) and water consumption (b) and polymerization of the layer (c) under water release. The final layer is crosslinked but is not necessarily linked regularly to the Si surface.

A study comparing different chlorosilanes ($CH_3SiH_nCl_{3-n}$ with n = 0-2) reveals clearly that when polymerization of the SAM layer occurs, as is, in particular, the case for n = 0, self-condensation is favored over surface reaction and a curing step is needed to complete the self-condensation and to undergo some surface reactions [40]. Without polymerization (n = 2), the SAM molecules attach to the surface as no competing process exists, but they are not crosslinked internally.

The preparation of an OTS layer on Si may proceed in the following steps [45, 46]: (i) HF dip to remove oxide layers from the Si surface; (ii) controlled chemical reoxidation in a 5:1:1 mixture of H,O : H,O, : NH, H at 70°C; (iii) rinsing with methanol and then the OTS solvent, for example, anhydrous toluene; (iv) immersion

into a 1% [44] or even less concentrated [31, 43, 47] solution of OTS in toluene, because the previously used mixtures of hexadecane and $CCl_4$, have been replaced for environmental reasons; (v) rinsing in pure toluene to remove excess OTS molecules and adsorbed layers from the surface; (vi) rinsing of the solvent from the surface with methanol; and (vii) drying/anneal at about 100-120°C for a few hours in nitrogen or vacuum. Alternatively, aging in air for a few days has been proposed [45]. When drying is performed in an oven under $N_2$, or vacuum, the OTS films are stable up to temperatures of about 400°C [46], which is not the case for samples annealed in air or oxygen. For oxide or silica surfaces, the first two steps may be skipped.

In the case of OTS, it is $–CH_3$, which is hydrophobic in nature and thus provides good antiwetting properties and has a low surface energy. Water contact angles of such films exhibit values up to 110° corresponding to a surface energy of 20 $mJ/m^2$ [46], which is comparable to commercial PTFE. Improvement is even possible with F-containing head groups or chains. Different fluorinated trichlorosilanes have been tested [31,45,46] that were developed mainly for antiadhesive coatings in micromechanical devices [48]. In the case of $-CF_3$, a F-terminated surface of the SAM exists with antiwetting properties better than PTFE characterized by surface energies of 5-12 $mJ/m^2$ [34,45].

Somewhat more complex are the Ormocers [49]. They consist of an organic-inorganic network linked to the surface and feature among other properties increased abrasion resistance. They are applicable in immersion to glass or polymers. Their basic antiwetting properties are somewhat lower than those of OTS with contact angles of 55° water. For these coatings, an admixture as low as 1% of a fluorinated compound was successful in increasing the contact angles by a factor of about 2, meeting the PTFE features. This improvement in functionality did not increase with

increasing admixtures and thus the abrasion resistance was not affected.

## 2.5 APPLICATIONS

Applications already demonstrated include diffractive optics, magnetic arrays, biosensors, quantum point contacts, single-electron transistors, (MESFETS), and interdigitated fingers. All benefit first from the capability to pattern large areas with small features and second the use of a polymer on a given substrate, thereby adding several benefits by choosing a polymer the properties of which may be enhanced by nano-structuring. For example, a polymer suitable for printing in the 10- to 100-nm scale spun on glass or plastic can be used as a low-cost biosensor, which can be disposed of after one use, thus minimizing contamination. Moreover, low-cost planar approaches are bound to become a growth area for the fabrication of lab-on-a-chip-based sensors in medical technologies. The flexibility offered by polymers is especially relevant because these can be made to react to different environments by building chemical, optical, mechanical, or electrical responses.

### *2.5.1 Biosensor*

One key aspect when considering the fabrication of biosensors is volume production. Montelius et al. [50] have shown that nanoimprint lithography is highly suited to fabricate interdigitated metal electrodes and contact pads with feature size of 100 nm and spacing varying from 100 to 500 nm. The authors tested the capacitance of about 17 pF and found that it did not vary significantly between 1 kHz and 1 MHz. Likewise, the 1-GΩ resistance between the fingers suggested there was no unwanted current on the surface. Future work includes the fabrication of biocompatible materials and site selectivity.

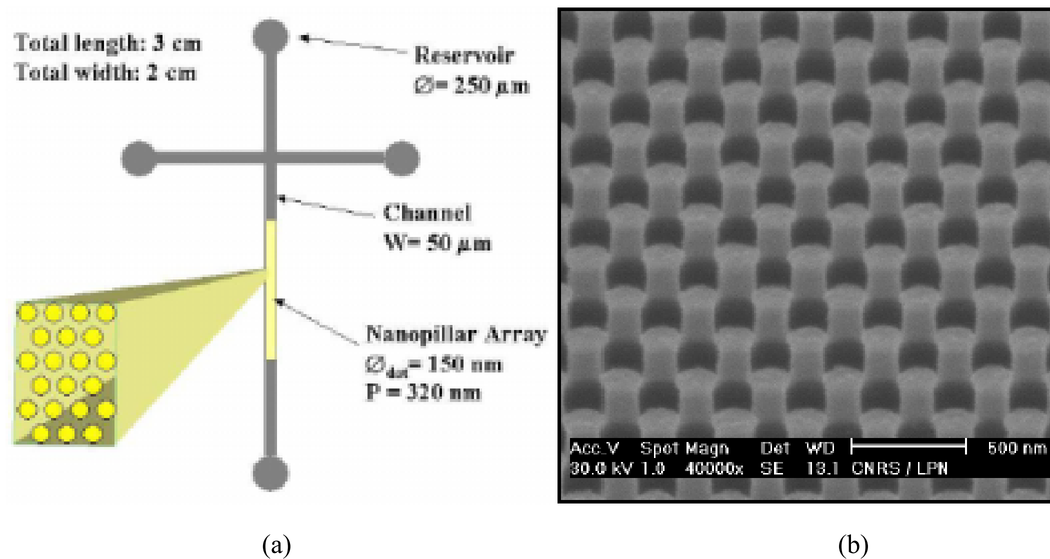


(a) (b)

**Figure 2-12.** (a) Schematic top view of the DNA electrophoresis microchip. (b) SEM displayed a portion of a nanopillar array replicated in SiO2/Si via tri-layer NIL for PCR reactors, mixing chambers, local electrokinetic fluid pumps integrated on the same chip.

Other representative work in this area is that of the Glasgow University team, who has explored patterning of glass and plastic surfaces for cell cultivation [31, 51, 52]. Typical electrophoresis microchip and nanopillar were given in Figure 2-12.

### *2.5.2 Photodetectors and Light Emitters*

The fact that printing can be carried out on a polymer spun on a silicon substrate, followed by standard lift-off techniques, leads to low-cost metal-semiconductor-metal (MSM) detectors. The pressure and temperature used in imprint lithography can be kept low enough to avoid degradation of the underlying CMOS [complementary MOSFET (metal-oxide-semiconductor field effect transistor)] platform. Yu et al. [53] have demonstrated MSM photodetectors with lines and spacing between 200 and 600 nm. The silicon mold had features between 193 and 330 nm high and patterned areas of 14 x 14 $\mu m^2$, which were printed on a PMMA coating the GaAs substrate as shown in Figure 2-13. Control MSM devices were fabricated by photolithography. As long as

the pressure during nanoimprinting was kept below 600 psi, the I-V curves revealed

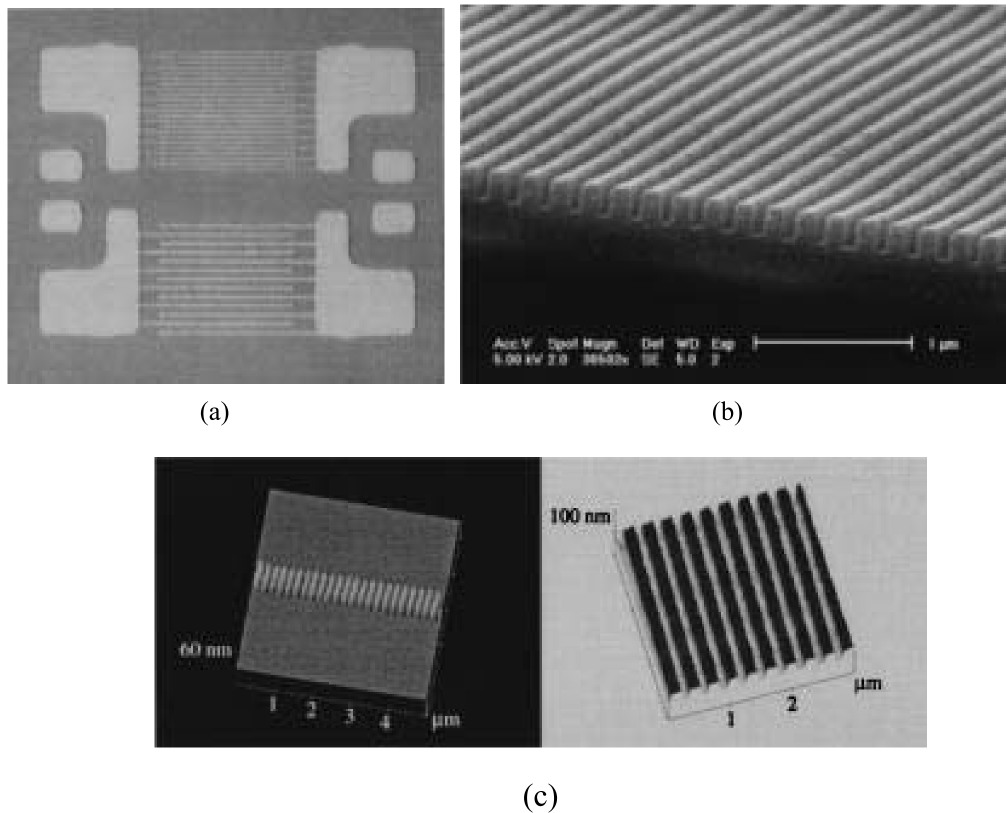


**Figure 2-13.** (a) GaAs MSM photodetectors with finger spacing of 300 and 600 nm, respectively, fabricated using nanoimprint lithography. (b) SEM image of the patterned grating of PMMA/$Alq_3$/DCMII with a period of 200 nm by nanoimprint. (c) AFM images of the $Alq_3$/DCMII gratings with a period of 200 nm (left) and 300 nm (right), respectively, patterned directly by nanoimprint.[53, 54]

no detectable device degradation. Small differences were ascribed to surface recombination. In principle, there is nothing on the way toward larger areas patterned with 60-nm features for even higher frequency operation.

## REFERENCES

1. L. R. Harriott, *Mater. Sci. Semicond. Process*. **1**, 93 (1998).

2. B. Michel; A. Bernard; A. Bietsch; E. Delamarche; M. Geissler; D. Juncker; H Kind; J. P. Renault; H. Rothuizen; H. Schmid; P. Schmidt-Winkel; R. Stutz; H. Wolf. *IBM J. Res. & Dev*. **45** 697 (2001).

3. Y. Xia; X. M. Zhao; G. M. Whitesides. *Microelectonr. Eng*. **32**, 255 (1996)

4. H.C. Scheer; H. Schulz; T. Hoffmann; in: H. S. Nalwa (Ed.) *Handbook of Thin Film Materials*, **5**, Academic Press, 1 (2002).

5. S. Y. Chou; P. R. Krauss; P. J. Renstrom. *Appl. Phys. Lett*. **67**, 3114 (1995).

6. S. Y. Chou; P. R. Krauss; P. J. Renstrom. *Science*, **272**, 85 (1996).

7. S. Y. Chou. *U.S. Patent* 5.772,905 (1998).

8. S. Y. Chou; P. R. Krauss; P. J. Renstrom. *J. Vac. Sci. Technol., B* **14**, 4129 (1996).

9. S.Y. Chou; P.R. Krauss; W. Zhang; L. Guo; L. Zhuang. *J. Vac. Sci. Technol. B*. **15**, 2897 (1997).

10. R. W. Jaszewski; H. Schift; J. Gobrecht; P. Smith. *Microelectron. Eng*. **41/42**, 575 (1998).

11. H. Schift; R. W. Jaszewski; C. David; J. Gobrecht. *Microelectron. Eng*. **46**,121 (1999).

12. J. Haisma; M. Verheijen; K. van den Heuvel; J. van den Berg. *J. Vac. Sci. Technol. B*. **14**, 4124 (1996).

13. R. Bartolini; W. Hannan; D. Karlsons; M. Lurie. *Appi. Opt*. **9**, 2283 (1970).

14. C. Puech; *Opt. Commun*. **7**, 135 (1973).

15. R. Ulrich; H. P. Weber; E. A. Chandross; W. J. Tomlinson; E. A. Franke. *Appl. Phys. Lett.* **20**, 213 (1972).

16. S. Y. Chou; P. R. Krauss. *Microelectron. Eng.* **35**, 237 (1997).

17. M. Li; J. Wang; L. Zhuang; S. Y. Chou. *Appl. Phys. Lett*. **76**, 673 (2000).

18. A. Lebib; Y. Chen; J. Bourneix; F. Careenac; E. Cambril; L. Couraud; H. Launois. *Microelectron. Eng.* **46**, 319 (1999).

19. R. W. Jaszewski; H. Schift; J. Gobrecht; P. Smith. *Microelectron. Eng.* **41/42**,575 (1998).

20. F. Gaboriau; M. C. Peignon; A. Barreau; G. Turban; C. Cardinaud; K. Pfeiffer; G. BleidieBel; G. Griitzner. *Microelectron. Eng*. **53**, 501 (2000).

21. H. Schuiz; H.C. Scheer; T. Hoffmann; C. M. Sotomayor Torres; K. Pfeiffer; G. Bleidiessel; G. Griitzner; B. Heidari. *J. Vac. Sci. Technol., B* **18**, 3582 (2000).

22. B. C. Wu; X. Y. Sun; W. Zhang; L. Zhuang; L. Kong; S. Y. Chou. *J. Vac. Sci. Technol. B* **16**. 3825 (1998).

23. H. C. Scheer; H. Schuiz; T. Hoffmann; C. M. Sotomayor Torres. *J. Vac. Sci. Technol..B* **16**, 3917 (1998).

24. K. Zimmer; K. Otte; A. Braun; S. Rudschuck; H. Friedrich; H. Schuiz; H. C. Scheer; F. Bigl. *Proc. EUSPEN.* **1**, 534 (1999).

25. K. Pfeiffer; G. Bleidiessel; G. Gnietzner; H. Schuiz; T. Hoffmann; H. C. Scheer; C. M. Sotomayor-Torres; J. Ahopelto. *Microelectron. Eng*. **46**,431 (1999).

26. F. Gaboriau; M. C. Peignon; A. Barreau; G. Turban; C. Cardinaud; K. Pfeiffer; G. BleidieBel; G. Griitzner. *Microelectron. Eng*. **53**, 501(2000).

27. K. Pfeiffer; M. Fink; G. Bleidiessel; G. Gruetzner; H. Schuiz; H. C. Scheer; T. Hoffmann; C. Cardinaud. *Microelectron. Eng.* **53**, 411 (2000).

28. S. Hector. *Microelectron. Eng.* **41/42**, 25 (1998).

29. B. Heidari; L. Maxirnov; L. Montelius. *J. Vac. Sci. Technol., B.* **17**, 2961 (1999).

30. B. G. Casey; D. R. S. Gumming; L. L. Khandaker, A. S. G. Curtis; C. D. W. Wilkinson. *Microelectron. Eng*. **46**, 125 (1999).

31. M. Colburn; S. Johnson; M. Stewart; S. Damie; T. Bailey; B. Choi; M. Wedlake; T. Michaelson; C. G. Willson. *Proc. SPIE,* **3676**, 379 (1999).

32 D. W. van Krevelen; Properties of Polymers, Elsevier, Amsterdam (1996).

33. K. N. G. Fuller; F. R. S. Tabor. *Proc. R. Soc. London. Ser. A,* **345**, 327 (1975).

34. M. Colburn; B. J. Choi; S. V. Sreenivasan; J. G. Ekerdt. *Electron, Ion and Photon Beam Technology and Nanofabrication EIPBN* (2000).

35. D. Y. Kwok; A. W. Neumann. *Adv. Colloid Interface Sci.* **81**, 167 (1999).

36. Y. Xia; X. M. Zhao; G. M. Whitesides. *Micmelectron. Eng*. 32. 255 (1996).

37. N. Roos; T. Luxbacher; T. Glinsner; K. Pfeiffer; H. Schuiz; H. C. Scheer. *Proc. SPIE,* **4343** (2001).

38. I. Martini; D. Eisert; S. Kuhn; M. Kamp; L. Worschech; J. Koeth; A. Forchel. *J. Vac. Sci. Technol., B* **18**, 3561 (2000).

39. C. P. Tripp; R. P. N. Veregin; M. L. Hair. *Langmuir,* **9**, 3518 (1993).

40. C. P. Tripp; M. L. Hair. *Langmair,* **11**, 149 (1995).

41. C. P. Tripp; M. L. Hair, *Langmuir*, **11**, 1215 (1995).

42. P. Silberzan; L. Leger; D. Ausserre; J. J. Benattar. *Langmuir,* **7**, 1647 (1991).

43. J. D. Le Grange; J. L. Markham. *Langmuir* **9**, 1749 (1993).

44. X. Zhao; R. Kopelman. *J. Phys. Chem*. **100,** 11014 (1996).

45. R. Maboudian; W. R. Ashurst; C. Carraro. *Sens. Actuators,* **82**. 21 (2000).

46. R. Maboudian; R. T. How. *J. Vac. Sci. Technol.. B* **15**, 1 (1997).

47. M. Goidmann; J. V. Davidovits; P. Silberzan. *Thin Solid Films*, **166**, 327 (1998).

48. M. C. B. A. Michielsen; V. B. Marriott; J. J. Ponjee; H. van der Wel; F. J. Touwslager; J. A. H. M. Moonen. *Microelectron. Eng*. **11**, 475, (1990).

49. K. H. Haas; S. Amberg-Schwab; K. Rose. *Thin Solid Films,* **351**, 198 (1999).

50. L. Montelius; B. Heidari; M. Graczyk; I. Maxirnov; E. L. Sarwe; T. G. I. Ling. *Micro- and Nano-Engineering 99 Conference*, **53**, 521 (2000).

51. P. M. Moran; F. F. Lange. *Appl. Phys. Lett*. **74**, 1332 (1999).

52. C. D. W. Wilkinson; A. S. G. Curtis; J. Crossan. *J. Vac. Sci. Technol B* **16,** 3132

(1998).

53. Z. Yu; J. Steven; J. Schablitsky; S. Y. Chou. *Appl. Phys. Lett*. **74**, 2381 (1999).

54. J. Wang; X. Sun; L. Chen; S. Y. Chou. *Appl. Phys. Lett*. **75**, 2767 (1999).